1-1-2007

Interaction of Water with Cap-Ended Defective and Non-Defective Small Carbon Nanotubes

J. L. Rivera

J. L. Rico

F. W. Starr
Wesleyan University

Recommended Citation
Jose L. Rivera, J. L. Rico, and Francis W. Starr. "Interaction of Water with Cap-Ended Defective and Non-Defective Small Carbon Nanotubes" Journal of Physical Chemistry C 111 (2007): 18899-18905.

Interaction of Water with Cap-Ended Defective and Nondefective Small Carbon Nanotubes

Jose L. Rivera,[†,‡] Jose L. Rico,[‡] and Francis W. Starr*[,†]

Department of Physics, Wesleyan University, Middletown, Connecticut 06459, and Department of Chemical Engineering, Universidad Michoacana de San Nicolás de Hidalgo, Morelia, Michoacán, 58000 México

Received: July 28, 2007; In Final Form: October 16, 2007

We present a theoretical study of the structure, local curvature angles, and reactivity of cap-ended (7,0), defective and nondefective carbon nanotubes. We find that the most reactive sites are the atoms that form part of the caps even when the Stone−Wales defect is present. Each carbon in the carbon nanotube is located at the top of a pyramidal structure with three walls of 5-, 6-, or 7-carbon rings. Among the carbons making up the caps, the most reactive sites are the top pyramidal atoms between two 5-carbon rings and one 6-carbon ring and each 5-carbon ring has attached another 5-carbon ring. The least reactive sites are the top pyramidal atoms between three 6-carbon rings. The activity of each pyramidal structure is strongly correlated to its local curvature angle. The dissociation of one water molecule on the surface of the carbon nanotubes confirms the location of the most active site. The dissociation of water produces a hydroxyl group and a hydrogen atom united each to two adjacent carbon atoms. The dissociation process of water on carbon nanotubes is energetically favorable starting from the isolated molecules.

I. Introduction

The interaction of water with surfaces has been the subject of study of numerous experimental and theoretical works due to the ubiquity and importance of water to physical and chemical phenomena on planar and curved surfaces.[1−4] Much is already known about water interactions with planar carbon surfaces. For example, theoretical calculations have shown that water does not wet planar and perfect carbon surfaces, such as crystalline graphite at room temperature.[5] The experimentally measured contact angle between water and graphite is presumably due to impurities and surface imperfections.[6−8] However, at higher temperatures theoretical calculations have predicted that water will wet the perfect surface of graphite.[5,9] At low and ambient temperatures, water reacts with carbon atoms that form the edges of graphite and dissociates.[10] The dissociated water molecules form hydroxyl groups that later act as active sites for physical adsorption processes.

Carbon nanotubes (CNs) are an ideal system in which to study water interactions with curved surfaces. Moreover CNs have numerous practical applications involving water, including nanofluidics[11−13] and fluid and ion separations.[14,15] The interaction of water with CNs has been the subject of many experimental[16−18] and theoretical[13,19−21] studies. Molecular simulations and experiments on water inside and outside CNs have demonstrated that water penetrates the cavities of the nanotubes[11,12,14,22] and that molecules and protons flow through the nanotubes with fast rates of transport.[12,23] Ellison et al.[16] experimentally studied the adsorption and dissociation of water on single-walled CNs using Fourier transform IR spectroscopy at room temperature. They concluded that a small number of water molecules dissociate and react with the nanotube forming carbon−oxygen and carbon−hydrogen bonds, whereas the majority of the water molecules adsorb to the surface without dissociating. Although the adsorption process occurs in the scale of hours, the dissociation reactions occur quickly at the beginning of the process. As in the case of dissociation and binding of water on graphite, dissociated molecules of water form hydroxyl bonded groups that act as active adsorption sites for incoming water molecules. First principles calculations of the dissociation of water have demonstrated that small carbon substrates made of graphene surfaces with vacancies behave like a catalyst during the dissociation reaction of water and the production of molecular hydrogen can be achieved.[24] The active sites for chemisorption and the dissociation processes predicted by these calculations can be already functionalized during the synthesis and purification of the nanoscale structures. An activation process should be arranged to produce the chemisorption and dissociation of molecules on these structures.[24,25]

Theoretical calculations using ab initio and density functional theory (DFT) methodologies have demonstrated that water in open and non-defective CNs adsorb at distances between 2.5 and 3.04 Å, with weak binding energies in the range of 0.035 and 0.143 eV.[19−21] The functionalization of the inner and outer surfaces of CNs[26−28] with groups containing oxygen in their structure modifies the amount of water adsorbed. In the presence of carboxylic groups, CNs can be filled with water molecules at pressures lower than the case with no functional groups. Thus, the modification of the inner and outer walls of CNs offers many possibilities to build new materials for scientific and technologic applications involving water and simple fluids.

Vacancies and Stone−Wales defects (SWDs) in CNs enhance the dissociative chemisorption and physisorption of molecular oxygen[29,30] and ozone,[31] but the physical or chemical adsorption process of water in the presence of SWD has not been evaluated. In this work, we examine the effects of SWDs on water adsorption of cap-ended CNs. We find that the most energetically favorable sites for water molecules to chemisorb at CNs surfaces are those sites close to the top of the caps, regardless of whether SWDs are present or not. Predictions based on electron population analysis on the isolated molecule of CNs

* To whom correspondence should be addressed.
[†] Wesleyan University.
[‡] Universidad Michoacana de San Nicolás de Hidalgo.

10.1021/jp075989r CCC: $37.00
Published on Web 12/06/2007

confirm these results. The dissociation of the water molecule forms hydroxyl and hydrogen functional groups in the outer surface of the CNs. We also find that the chemisorption activity of each site is related to its local curvature. We report the results for geometry optimizations and energetics of (7,0) cap-ended defective and nondefective CNs in section II of this paper. We present the study of reactivity, local curvature angles and its relationship in section III. We discuss the energies for chemisorption processes of water on CNs and its final conformations in section IV. Finally, we present the conclusions of this work in section V.

II. Electronic Structure

We obtain the most stable conformations of the CNs and water molecules through energy minimizations using ab initio calculations. These optimized structures are used later to calculate the energies for the chemisorption processes. The optimized structure of the cap-ended (7,0) nondefective CN was obtained using the GAMESS code[32] at the HF/3-21G* level of theory. The size of the basis set we use for the geometry optimization produces accurate results for the most stable conformation of the molecule.[33] We show snapshots of the optimized structure in Figure 1a−d. The structure contains four slabs of 6-carbon rings (6-CR) forming the cylinder of the CN. The CN is cap-ended at both ends using a nonsymmetrical cap composed of five 5-CR and one 6-CR forming one slab of rings at each end with a 6-CR at the top of the cap.[34] Starting with the (7,0) nondefective CN structure, we obtain a second structure with a SWD[35] by rotating one of the bonds and perform an additional energy minimization at the same level of theory. The SWD is characterized by the rotation of one bond to produce two 5-CR and two 7-CR, as shown in the center of Figure 1e.

The structures of both the nondefective and defective CNs are not perfect cylinders because of the nonsymmetrical caps used and the SWD. The structures have the approximate form of a peanut, and the center of the cylinder does not form a perfect circle. If we define an axial axis as the vector crossing the center of mass of the two 6-CR at the top of both caps, the axial length of the nondefective CN is 11.369 Å, whereas the defective has a length of 11.476 Å. The thinnest and widest diameters of the CNs were measured as the smallest and largest separation among all of the possible pairs of opposite carbons located at the central slabs of the CNs. For the nondefective CN, the diameters are 5.259 and 5.536 Å, whereas for the defective CN, the diameters are 5.052 and 5.611 Å, respectively. If we compare the structures, the nondefective CN is closer to a perfect cylinder than the defective CN. Although those tubes are narrower than most commonly synthesized CNs, single-walled and multi-walled, cap-ended CNs with diameters as thin as 4 Å can be synthesized on templates of $AlPO_4$-5 zeolites[36] and arc discharge methods.[37]

We obtain total energies through DFT calculations at the B3LYP/6-31G* level of theory; we find that the nondefective CN has an energy 2.77 eV lower than the defective CN. This difference in total energies can be predicted for open and infinite CNs with chiral conformation (*m*,*n*), through the empirical expression developed by Zhou and Shi using semiempirical methods[38]

$$E_{SW} = E^0_{SW} + a_0 e^{-b_0 r} + \frac{c_0}{r^2} \quad (1)$$

$$r = \sqrt{3}\, a_C (m^2 + n^2 + mn)^{1/2}/2\pi \quad (2)$$

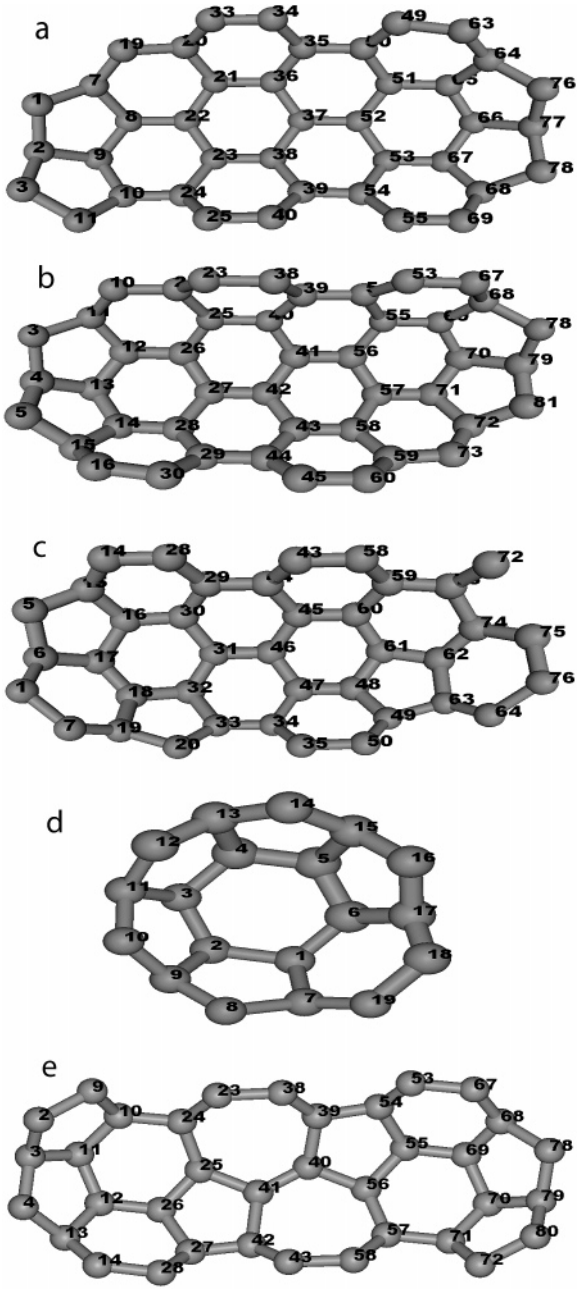

Figure 1. Snapshots of the structures of the (7,0) nondefective and defective CNs. The front of the nanotube is not shown and only carbons in the back of the structures are drawn. Structures a−c are for the nondefective nanotube and they represent rotations of 120° in the axial axis. Structure d represents the top of the cap. Structure e represents the structure of the defective CN with the SWD.

where E_{SW} is the energy necessary to rotate one bond in a nondefective and open CN to produce a defective CN with a SWD. *r* is the radius of the CN. a_C is the bond distance in the CN. For (*m*,0) nantubes: $E^0_{SW} = 6.02$ eV, $a_0 = -1.58$ eV, $b_0 = 0.0451$ Å^{-1}, and $c_0 = -18.74$eV Å^2. For a (7,0) CN, expression (1) results in $E_{SW} = 1.20$ eV, less than half the value found in our work. The difference between the values is probably due to the effect of the cap, which is not considered in expression 1. DFT calculations of the formation of SWD on infinite (10,0) CN show good agreement with expression 1.[31] The DFT calculations model the infinite CN as a unit crystalline cell under periodic conditions. Nevertheless, E_{SW} decreases from 4.1 to 3.7 eV when the number of atoms increases from 80 to 120. If the same trend continues for larger number of atoms in the unit

cell, the value of E_{SW} will be closer to the results of this work for small CNs.

III. Reactivity

The reaction between two or several species is traditionally studied through the frontier molecular orbital theory and molecular electrostatic potential. An alternative methodology is the Fukui function, which produces a trend of intrinsic reactivity for each site in the molecule without explicitly studying the final product.[39] The Fukui function has the advantage that it is computationally much less demanding, particularly as the molecule size increases. The Fukui function measures the intrinsic reactivity obtained for each site in the molecule. Values of the Fukui function can only be compared with other sites within the same molecule. The Fukui function has been employed previously in the study of systems with delocalized charges, such as those present in CNs.[40−42] We estimate the reactivity of the CNs using the condensed Fukui functions[43]

$$f_i^+ = -\{q_i(N+1) - q_i(N)\} \quad (3)$$

$$f_i^- = -\{q_i(N) - q_i(N-1)\} \quad (4)$$

$$f_i^0 = -1/2\{q_i(N+1) - q_i(N-1)\} \quad (5)$$

which are related to the nucleophilic, electrophilic, and radical attacks, respectively. q_i is the partial charge of atom i, which can be obtained through a Mulliken gross population analysis.[44] N, $N-1$, and $N+1$ indicate evaluations of the partial charges at the ground state and the corresponding anionic and cationic states, respectively. We carry out DFT calculations at the B3LYP/6-31G* level of theory using the optimized geometries for the defective and nondefective CNs to obtain the Mulliken partial charges. The basis set we use for the single-point calculation of the energy produces reliable results of the electronic density of the molecule.[33] Previous calculations of adsorption energies of oxygen and carbon monoxide on carboneous surfaces show that the deviation of the results using the HF/3-21G* for geometry optimizations and B3LYP/6-31G* for energy calculations are ∼5% compared to the calculations using B3LYP/6-31G* for both geometry optimizations and energy calculations.[45] We are able to use a larger basis set for the energy calculations than for geometry optimizations because the energy calculations are less computationally taxing.

Previous theoretical calculations on the activity of infinite or small and open CNs with defects have shown that the most active carbon atoms for physical and chemical adsorption processes are those belonging to defects in the CN structure,[29,31,46] but the calculation of the activity for atoms belonging to the cap of the CN was not performed because caps were not present in the studied structures.

III.1. Nondefective CN. Figure 2 shows the reactivity determined by the three Fukui functions as a function of the atom number for the non-defective CN calculated using expressions 3−5. Atoms are numbered consecutively; we plot only half of the atoms because of the symmetry of the CN. The figure is divided into 4 regions corresponding to the atoms that form the top of the cap (I) and the atoms between two consecutive slabs of rings (II− IV). Carbon atoms in region II form part of the slab of rings belonging to the cap and they also form part of the first slab of rings with 6 carbon atoms. Atoms in region I have uniform reactivity, and there is almost no difference among nucleophilic, electrophilic, and radical attacks. In region

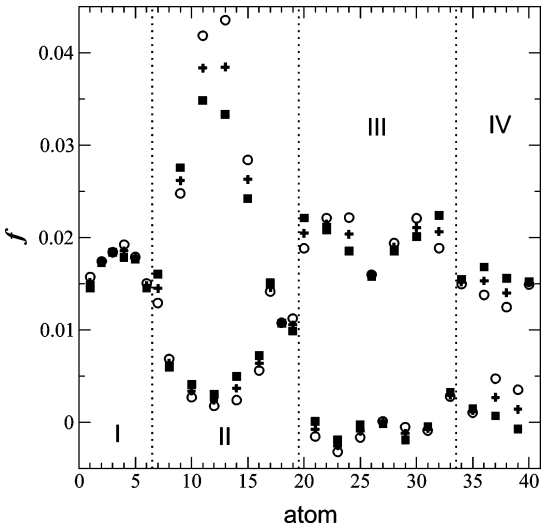

Figure 2. Fukui functions vs carbon atom number for the (7,0) nondefective CN. Circles, crosses, and squares represent f_i^+, f_i^- and f_i^0, respectively. Region I contains atoms belonging to the top of the CN. Regions II−IV contain atoms between consecutive slabs of rings.

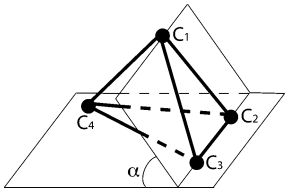

Figure 3. Scheme of one of three possible values for the pyramidalization angle of atom C_1 between planes $C_1-C_2-C_3$ and $C_2-C_3-C_4$.

II, for carbons C_7 through C_{17}, we find sets of intercalated weakly and highly reactive atoms. Carbons C_{11} and C_{13} of region II are the most reactive atoms, especially for nucleophilic attacks. Regions III and IV show a similar behavior to region II, but for this region of the molecule, weakly reactive carbon atoms are intercalated between moderately reactive atoms. These results suggest that the most reactive atoms of the CN should be those at the cap of the CN.

Lin et al.[47] have studied the reaction of methylamine addition on CNs using DFT methodology. They found that the reactivity of the sites depends on its pyramidalization angle, which is related to the local curvature of the site. The carbons with highest angles were those containing two 5-CR and one 7-CR. We define the pyramidalization angle in Figure 3, which shows a carbon atom, C_1, which is bonded to three other carbon atoms C_2-C_4 forming a pyramid, with the C_1 carbon on the top of the pyramid. The pyramidalization angle α is defined as the angle between the base plane and the plane of a face of the pyramid, and it has three values, depending on which face of the pyramid is used to calculate the angle. In graphite, all atoms have a hybridization sp^2 and thus all angles $\alpha = 0°$, whereas for the hybridization sp^3, e.g., methane, all angles $\alpha = 32.25°$. Due to the curvature of the wall in CNs, angles $\alpha \neq 0°$ and depends on the diameter of the CN. For carbons belonging to the cap of the CN, the values of α are higher than those for the carbons belonging to the center of the CN due to the greater curvature of the cap.

We calculate the local curvature angle, $\langle\alpha\rangle$, as the average of the three possible values of α for each carbon site and parametrically plot the three reactivities as a function of $\langle\alpha\rangle$ (Figure 4) for the (7,0) nondefective CN. We find that $10.6° < \langle\alpha\rangle < 35.6°$, as found in the study of Lin et al.[47] More importantly, the most and least reactive atoms correspond to

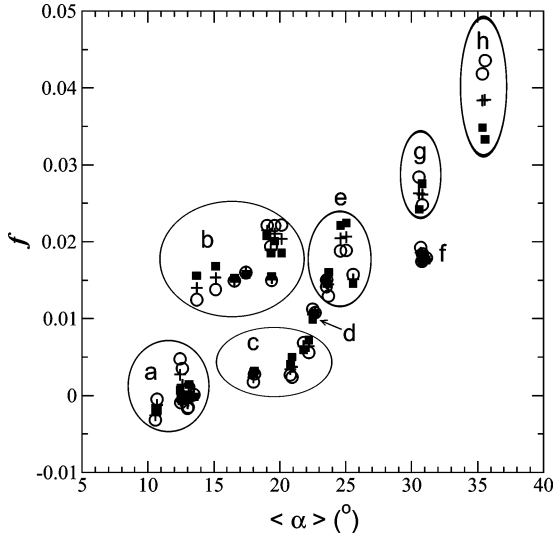

Figure 4. Fukui functions vs ⟨α⟩ for the (7,0) nondefective CN. Symbols are the same as in Figure 2. Letters a−h refer to substructures of Figure 5.

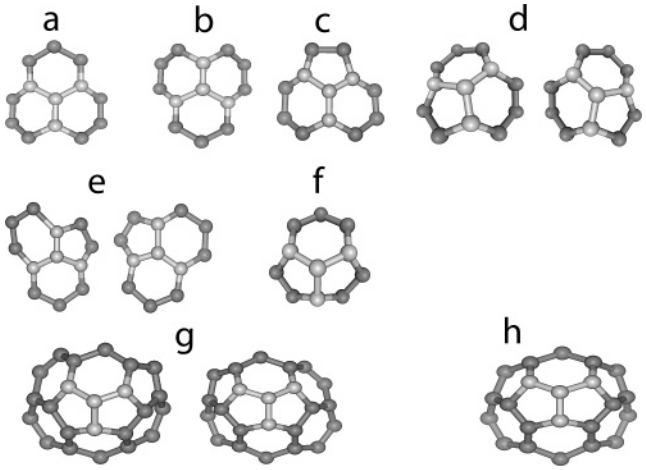

Figure 5. Snapshots of all possible pyramidal structures of the (7,0) nondefective CN. All of the structures are oriented to the top of the CN. The structures are formed by walls of (a) three 6-CR (one 6-CR at the top), (b) three 6-CR (two 6-CR share the top), (c) one 5-CR and two 6-CR (one 5-CR at the top), (d) one 5-CR and two 6-CR (one 6-CR at the top), (e) one 5-CR and two 6-CR (one 6-CR and the 5-CR share the top), (f) two 5-CR and one 6-CR (the 6-CR at the top), (g) two 5-CR and one 6-CR (the 6-CR at the top, and there is one 5-CR outside of the pyramidal structure bonded to one 5-CR of the pyramidal structure), and (h) two 5-CR and one 6-CR (the 6-CR at the top, and there is one 5-CR outside of the pyramidal structure bonded to each 5-CR of the pyramidal structure).

those with largest and smallest local curvature angles, respectively. The CN we study contains several pyramidal substructures formed by the combination of 5-CR, 6-CR, and 7-CR. For a specific pyramidal substructure, several orientations of the member CR with respect to the top of the CN can be present. For example, if we have a pyramidal substructure formed by two 6-CR and one 5-CR, this structure can be repeated in the nanotube. Sometimes one 6-CR can be located aligned to the top of the same substructure, and sometimes one 5-CR can be located aligned to the top. Figure 5 shows all possible substructures, which are depicted with its actual orientation to the top of the CN. Substructures a and b are formed by three 6-CR, and they have different orientations with respect to the top of the CN and have different local curvature angles. For the substructure a, $10.6° < \langle\alpha\rangle < 13.7°$, whereas for substructure

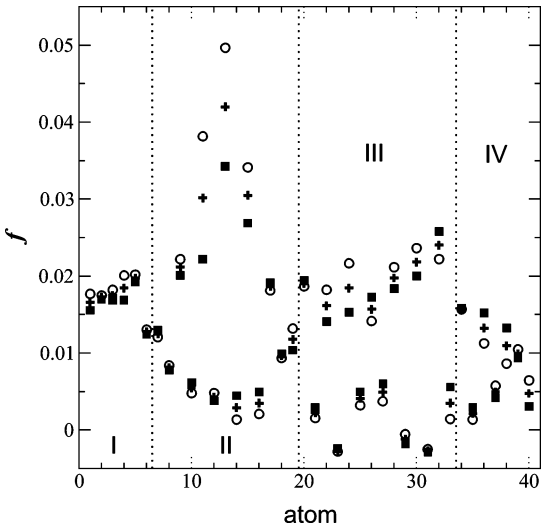

Figure 6. Fukui functions vs carbon atom number for the (7,0) defective CN. Symbols and regions I− IV represent the same as in Figure 2.

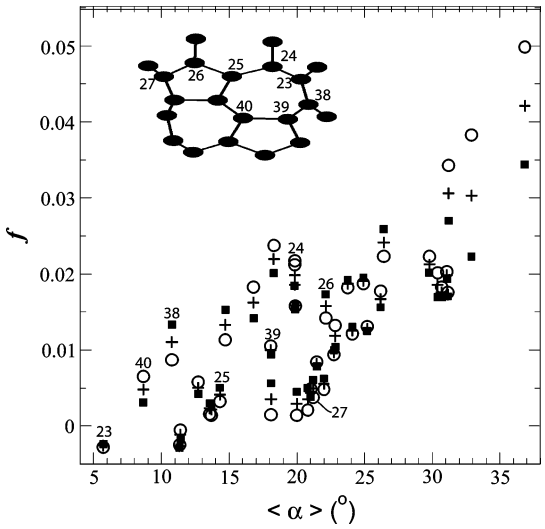

Figure 7. Fukui functions vs ⟨α⟩ for the (7,0) defective CN. Symbols are the same as in Figure 2. The inside snapshot represent the structure and numbering of carbons belonging to the SWD.

b, $13.7° < \langle\alpha\rangle < 20.3°$. The labeled grouped points in Figure 4 can be associated with the central atoms in the substructures of Figure 5. Central carbon atoms in substructures containing four consecutive 5-CR are the most reactive sites with ⟨α⟩ values similar to those found in hybridizations sp^3. Central carbon atoms in substructures containing three 6-CR with one of the rings orientated to the top of the CN have the smallest reactivity. The second most reactive carbons are those central atoms in substructures containing three consecutive 5-CR, such as those shown in substructure g. Substructures similar to those used in the work of Lin et al.[47] showed moderate or low reactivity. Comparing substructures with the same type of rings but with different orientations relative to the top, as in substructures a and b, the reactivity is also different. The Fukui functions for substructure b are larger than those for substructure a. The same trend is found between substructures c−e, which are formed by one 5-CR ring and two 6-CR. Substructure c, which has the 5-CR in the top of the substructure, shows the smallest ⟨α⟩ and reactivity, whereas substructure e, where the 5-CR shares equally the top of the substructure with a 6-CR, shows the largest ⟨α⟩ and reactivity values. Substructure d is an intermediate rotated substructure between substructures c and e, also show interme-

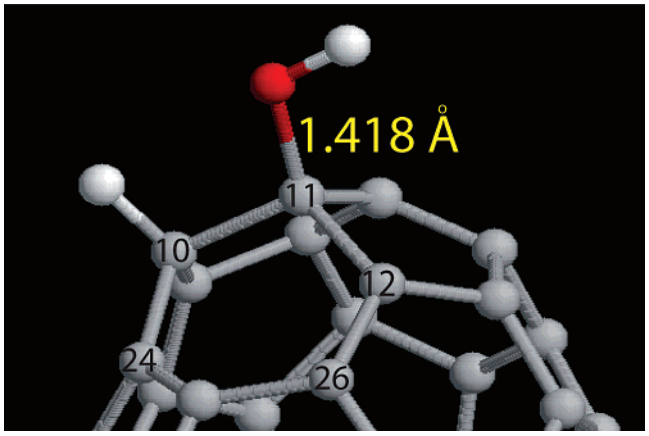

Figure 8. Snapshot of the optimized structure of dissociated water on the (7,0) nondefective CN.

diate $\langle\alpha\rangle$ and reactivity values. In short, we find a strong correlation between local curvature angles and site reactivity, and there is also a strong correlation between the chemical bonding of the pyramidal substructures and its local curvatures angles.

III.2. Defective CN. We next focus our attention on how the SWD affects reactivity and curvature in the defective CN. We show the Fukui functions for the first 40 carbon atoms of the defective CN in Figure 6. The reactivity for the three types of attack is qualitatively similar to that of the nondefective CN. Region I is characterized by carbon atoms with moderate and uniform reactivity for the three types of attack. Some of the carbons belonging to region II are the most reactive, with an enhanced reactivity, especially for the nucleophilic attacks. Regions III and part of IV contain carbon atoms with moderate reactivity intercalated with atoms with low reactivity. The most reactive atoms are the carbons C_{11} and C_{13}. Hence, although atoms in the SWD have larger reactivity than their counterparts in the nondefective tube, the most reactive atoms are still those at the cap of the CN.

We show reactivity as a function of $\langle\alpha\rangle$ for the defective CN in Figure 7. Compared to the nondefective CN, $\langle\alpha\rangle$ in the defective CN is smaller for carbons C_{23} and C_{40} atoms, which belong to the SWD. The most reactive carbons are C_{11} and C_{13}, which belong to the cap of the defective CN; they also have the largest $\langle\alpha\rangle$. Overall, we find the same trend that carbon atoms with the smallest $\langle\alpha\rangle$ have small reactivity, whereas carbon atoms with the largest $\langle\alpha\rangle$ have the largest reactivity. Of the sixteen carbon atoms that form the SWD, the maximum $\langle\alpha\rangle$ is for carbon C_{26}, which has a pyramidal substructure, composed of one 5-CR and two 6-CR. The reactivity of atoms belonging to the SWD also has intermediate values. Carbon C_{24} has the maximum reactivity among the atoms of the SWD, which has a pyramidal substructure, composed of one 7-CR and two 6-CR. Thus, the introduction of the SWD enhances both reactivity and local curvature angles compared to the nondefective tube but do not exceed the largest values associated with the atoms at the cap of the tube.

IV. Chemisorption of Water

In order to verify the prediction of the Fukui functions for the most active carbon sites, we carry out several energy minimizations with a water molecule dissociated at several sites of the nondefective CN. We perform the calculations at the HF/3-21G* and obtain the optimized geometries. The dissociation of water for the nondefective CN results in a hydroxyl group and a hydrogen atom each bonded to the adjacent carbons C_{11} and C_{10}, respectively, as shown in the snapshot of Figure 8. The final structure shows typical carbon−oxygen (1.418 Å), oxygen−hydrogen (0.967 Å), and carbon−hydrogen (1.089 Å) distances, similar to those obtained in the phenol molecule, which also contains a hydroxyl group and hydrogen atoms bonded to a 6-carbon aromatic ring.[48] For comparison, dissociated water on graphite surfaces with vacancies show a similar carbon−oxygen distance, ∼1.4 Å, through a large exothermic energy, 1.6 eV.[49] The dihedral angles $H-C_{10}-C_{11}-O$ (4.49°) and $H-O-C_{11}-C_{10}$ (173.00°) reflect an alignment of the hydrogen atoms to the plane $C_{10}-C_{11}-O$ as shown in the snapshot of Figure 8. Similar calculations with the defective CN produce a similar structure with the same bond distances and dihedral angles $H-C_{10}-C_{11}-O$ (5.79°) and $H-O-C_{11}-C_{10}$ (175.47°), reflecting a better alignment of hydrogen atoms to the plane $C_{10}-C_{11}-O$. Previous studies without end capping did not search for the possibility of dissociated water states.

We further consider the possibility of chemisorption to neighboring sites. Specifically, we study the molecular geometry of the other possible products of dissociated water at the adjacent carbon pairs (C_3-C_{11} and $C_{12}-C_{11}$) on each nanotube. Additionally, we study the molecular geometry of the products of dissociated water on the CNs at C_{10} and all possible adjacent pairs for the nondefective tube. For the defective CNs, we consider the molecular geometry of the products of dissociated water at C_{24} and all possible adjacent pairs. We report the optimized geometries on Table 1. Carbon−oxygen bond distances are in the range of 1.412−1.447 Å, oxygen−hydrogen bond distances are in the range of 0.966−0.968 Å, and carbon−hydrogen bond distances are in the range of 1.078−1.089 Å, which are very close to the distances present in the phenol molecule.[48] More important are the binding energies, which we next report.

TABLE 1: Optimized Geometries and Energetics of Dissociated Water on Defective and Nondefective (7,0) Carbon Nanotubes

nanotube	pair of carbons	d_{C-C} (Å)	d_{C-O} (Å)	d_{O-H} (Å)	d_{C-H} (Å)	$\langle\alpha\rangle_{C-H}$ (°)	$\langle\alpha\rangle_{C-O}$ (°)	E_b (eV)
nondefective	$-O-C_{11}-C_{10}-H$	1.566	1.417	0.967	1.089	34.223	41.871	0.60
	$-O-C_{11}-C_3-H$	1.598	1.420	0.967	1.079	42.548	42.447	0.67
	$-O-C_{11}-C_{12}-H$	1.571	1.415	0.967	1.086	35.355	42.160	0.88
	$-O-C_{10}-C_{11}-H$	1.564	1.434	0.967	1.078	40.901	36.385	0.54
	$-O-C_{10}-C_{13}-H$	1.574	1.447	0.967	1.078	40.749	35.961	0.81
	$-O-C_{10}-C_{24}-H$	1.559	1.428	0.967	1.081	33.061	39.776	−0.12
defective	$-O-C_{11}-C_{10}-H$	1.568	1.418	0.967	1.089	35.869	41.613	0.41
	$-O-C_{11}-C_3-H$	1.588	1.412	0.968	1.081	42.806	43.379	1.03
	$-O-C_{11}-C_{12}-H$	1.594	1.416	0.967	1.085	35.664	42.068	0.99
	$-O-C_{24}-C_{23}-H$	1.641	1.444	0.968	1.081	34.832	31.363	−0.16
	$-O-C_{24}-C_{25}-H$	1.656	1.436	0.967	1.090	24.277	34.280	−0.80
	$-O-C_{24}-C_{10}-H$	1.601	1.437	0.966	1.081	36.382	35.065	−0.02

We calculate the dissociative chemisorption energies as

$$E_b = (E_{nanotube} + E_{water}) - E_{complex} \quad (6)$$

where $E_{complex}$ is the energy of the complex in the chemisorbed state, $E_{nanotube}$ is the energy of the isolated CN, and E_{water} is the energy of an isolated water molecule. We obtain the energies through DFT calculations at the B3LYP/6-31G* level of theory. The chemistorption energies show energetically favorable processes for most of the sites, except for the products using the adjacent pair of carbons $C_{10}-C_{24}$ on the nondefective CN, and the products involving the C_{24}, which belongs to the SWD. For the nondefective CN, favorable E_b are in the range of 0.54−0.88 eV, whereas for the defective CN, favorable E_b are in the range of 0.41−1.03 eV. The carbon atoms belonging to the SWD show energetically unfavorable binding energies because they are less strained (low pyramidalization angle) than carbon atoms belonging to the cap of the CNs. The largest binding energy for the chemisorption of water on the defective CN is ~60% of the dissociation energy on graphite with vacancies.[49] These results demonstrate that the end caps at our CNs are more reactive with water than the sites along the main body of the tube, even when there is a SWD present. Additionally, the binding results support the predictions for the most reactive sites made using the Fukui function.

V. Conclusions

The reactivity of specific sites in (7,0) cap-ended, nondefective, and defective CNs can be predicted through an analysis of electron populations and using the Fukui functions. The results showed that carbon atoms belonging to the cap are more reactive that those belonging to the cylinder of the nanotube, even if there is a defect in the cylinder, as in the case of the SWD studied in this work. The SWD does have some effect; some of the carbons belonging to the SWD are more reactive than the rest of the carbons in the cylinder. The CNs studied are formed by several substructures characterized by a central atom in the top of a pyramid with walls composed of 5-CR, 6-CR, and 7-CR. Each substructure showed specific local curvature and reactivity when the orientation with respect to the top is also considered. Local curvatures angles in the range of 10.5°−35.6° for the nondefective CN and 5.7°−36.9° for the defective CN were obtained. Central atoms in substructures formed with two 5-CR and one 6-CR but also containing four consecutive 5-CR are the most reactive sites, while those formed by three 6-CR are the least reactive as shown in Figure 5. Within the SWD, the central atoms with substructures containing two 6-CR and, one 5-CR, or one 7-CR are the most reactive.

The dissociation of water on (7,0) cap-ended, defective, and nondefective CNs is energetically favorable starting from the isolated molecules. The chemisorption energies for the studied sites confirm the predictions of the Fukui function for the reactivity of the sites. The reaction on the nondefective CN produces a more stable product. The favorable energy for dissociation of water suggests that water in such nanoscale environments will spontaneously modify and functionalize CN surfaces. Such functionalization will be a disadvantage for applications involving very specialized nanodevices where the nanotube surfaces are dedicated to very specific tasks, but it will open new possibilities for new surfaces and applications at the nanoscale.

Future work will involve the study of complexes between carbon nanotubes and water molecules through physical interactions. Water forms weak covalent bonds in molecularly adsorbed states at alumina surfaces and graphite edges prior the chemisorption process. We will verify if a molecular adsorption also occurs at the nanotube surface, its nature, and implications on the following chemisorption processes. In this work, we study short carbon nanotubes in the scale of nanometers, whereas most of the synthesized nanotubes are in the scale of micrometers. In the future, we will study larger nanotubes with less expensive computational methodologies. Larger nanotubes will allow us to study the effect of the position of the defect with respect to its separation from the cap of the nanotubes, which can affect the activity of the defects in short nanotubes.

Acknowledgment. We thank the National Science Foundation for support under Grant No. DMR-0427239. We also thank Universidad Michoacana de San Nicolás de Hidalgo (México) and CONACYT (México) for support under Grant No. 48568.

References and Notes

(1) Raschke, T. M. *Curr. Opin. Struct. Biol.* **2006**, *16*, 152.
(2) Parks, G. A. *Rev. Mineral.* **1990**, *23*, 133.
(3) Wong, H. C.; Umehara, N.; Kato, K. *Wear* **1998**, *218*, 237.
(4) Vogler, E. A. *Adv. Colloid Interface Sci.* **1998**, *74*, 69.
(5) Gatica, S. M.; Johnson, J. K.; Zhao, X. C.; Cole, M. W. *J. Phys. Chem. B* **2004**, *108*, 11704.
(6) Fowkes, F. M.; Harkins, W. D. *J. Am. Chem. Soc.* **1940**, *62*, 3377.
(7) Luna, M.; Colchero, J.; Baro, A. M. *J. Phys. Chem. B* **1999**, *103*, 9576.
(8) Miura, K.; Morimoto, T. *Langmuir* **1991**, *7*, 374.
(9) Zhao, X.; Johnson, J. K. *Mol. Simulat.* **2005**, *31*, 1.
(10) Kelemen, S. R.; Freund, H.; Mims, C. A. *J. Vac. Sci. Technol. A* **1984**, *2*, 987.
(11) Sholl, D. S.; Johnson, J. K. *Science* **2006**, *312*, 1003.
(12) Holt, J. K.; Park, H. G.; Wang, Y. M.; Stadermann, M.; Artyukhin, A. B.; Grigoropoulos, C. P.; Noy, A.; Bakajin, O. *Science* **2006**, *312*, 1034.
(13) Striolo, A. *Nano Lett.* **2006**, *6*, 633.
(14) Kalra, A.; Garde, S.; Hummer, G. *Proc. Natl. Acad. Sci. U.S.A.* **2003**, *100*, 10175.
(15) Park, J. H.; Sinnott, S. B.; Aluru, N. R. *Nanotechnology* **2006**, *17*, 895.
(16) Ellison, M. D.; Good, A. P.; Kinnaman, C. S.; Padgett, N. E. *J. Phys. Chem. B* **2005**, *109*, 10640.
(17) Sharma, S. C.; Singh, D.; Li, Y. *J. Raman Spectrosc.* **2005**, *36*, 755.
(18) Engtrakul, C.; Davis, M. F.; Gennett, T.; Dillon, A. C.; Jones, K. M.; Heben, M. J. *J. Am. Chem. Soc.* **2005**, *127*, 17548.
(19) Peng, S.; Cho, K. J. *Nanotechnology* **2000**, *11*, 57.
(20) Zhao, J. J.; Buldum, A.; Han, J.; Lu, J. P. *Nanotechnology* **2002**, *13*, 195.
(21) Pati, R.; Zhang, Y.; Nayak, S. K.; Ajayan, P. M. *Appl. Phys. Lett.* **2002**, *81*, 2638.
(22) Wan, R. Z.; Li, J. Y.; Lu, H. J.; Fang, H. P. *J. Am. Chem. Soc.* **2005**, *127*, 7166.
(23) Mann, D. J.; Halls, M. D. *Phys. Rev. Lett.* **2003**, *90*, 195503.
(24) Kostov, M. K.; Santiso, E. E.; George, A. M.; Gubbins, K. E.; Nardelli, M. B. *Phys. Rev. Lett.* **2005**, *95*, 136105.
(25) Kuznetsova, A.; Mawhinney, D. B.; Naumenko, V.; Yates, J. T.; Liu, J.; Smalley, R. E. *Chem. Phys. Lett.* **2000**, *321*, 292.
(26) Rivera, J. L.; McCabe, C.; Cummings, P. T. *Nano Lett.* **2002**, *2*, 1427.
(27) Striolo, A.; Chiavo, A. A.; Cummings, P. T.; Gubbins, K. E. *J. Chem. Phys.* **2006**, *124*, 074710.
(28) Zhao, J. J.; Park, H. K.; Han, J.; Lu, J. P. *J. Phys. Chem. B* **2004**, *108*, 4227.
(29) Grujicic, M.; Cao, G.; Singh, R. *Appl. Surf. Sci.* **2003**, *211*, 166.
(30) Grujicic, M.; Cao, G.; Rao, A. M.; Tritt, T. M.; Nayak, S. *Appl. Surf. Sci.* **2003**, *214*, 289.
(31) Picozzi, S.; Santucci, S.; Lozzi, L.; Valentini, L.; Delley, B. *J. Chem. Phys.* **2004**, *120*, 7147.
(32) Schmidt, M. W.; Baldridge, K. K.; Boatz, J. A.; Elbert, S. T.; Gordon, M. S.; Jensen, J. H.; Koseki, S.; Matsunaga, N.; Nguyen, K. A.; Su, S. J.; Windus, T. L.; Dupuis, M.; Montgomery, J. A. *J. Comput. Chem.* **1993**, *14*, 1347.
(33) Foresman, J. B.; Frisch, A. *Exploring Chemistry with Electronic Structure Methods: A Guide Using Gaussian*, 2nd ed.; Gaussian Inc.: Pittsburgh, PA, 1995.
(34) Lair, S. L.; Herndon, W. C.; Murr, L. E.; Quinones, S. A. *Carbon* **2006**, *44*, 447.
(35) Stone, A. J.; Wales, D. J. *Chem. Phys. Lett.* **1986**, *128*, 501.

(36) Wang, N.; Tang, Z. K.; Li, G. D.; Chen, J. S. *Nature* **2000**, *408*, 50.
(37) Qin, L. C.; Zhao, X. C.; Hirahara, K.; Miyamoto, Y.; Ando, Y.; Iijima, S. *Nature* **2000**, *408*, 50.
(38) Zhou, L. G.; Shi, S. Q. *Appl. Phys. Lett.* **2003**, *83*, 1222.
(39) Parr, R. G.; Yang, W. T. *J. Am. Chem. Soc.* **1984**, *106*, 4049.
(40) Lopez, P.; Mendez, F. *Org. Lett.* **2004**, *6*, 1781.
(41) Nguyen, L. T.; De Proft, F.; Amat, M. C.; Van Lier, G.; Fowler, P. W.; Geerlings, P. *J. Phys. Chem. A* **2003**, *107*, 6837.
(42) Gomez, B.; Martinez-Magadan, J. M. *J. Phys. Chem. B* **2005**, *109*, 14868.
(43) Yang, W.; Mortier, W. J. *J. Am. Chem. Soc.* **1986**, *108*, 5708.
(44) Mulliken, R. S. *J. Chem. Phys.* **1955**, *23*, 1833.
(45) Montoya, A.; Mondragon, F.; Truong, T. N. *Carbon* **2002**, *40*, 1863.
(46) Lozzi, L.; Picozzi, S.; Armentano, L.; Valentini, L.; Kenny, J. M.; La Rosa, S.; Coreno, M.; de Simone. M.; Delley, B.; Santucci, S. *J. Chem. Phys.* **2005**, *123*, 034702.
(47) Lin, T. T.; Zhang, W. D.; Huang, J. C.; He, C. B. *J. Phys. Chem. B* **2005**, *109*, 13755.
(48) Ishiuchi, S.; Fujii, M.; Robinson, T. W.; Miller, B. J.; Kjaergaard, H. G. *J. Phys. Chem. A* **2006**, *110*, 7345.
(49) Allouche, A.; Ferro, Y. *Carbon* **2006**, *44*, 3320.